Weight Windows – an Improved Approach

Itzik Cohen
Dept. of Electrical Engineering - Systems
Tel Aviv University, Tel Aviv, Israel
Elbit Systems (Elisra), Bnei Brak, Israel
bitzikc@gmail.com

Nadav Levanon
Dept. of Electrical Engineering - Systems
Tel Aviv University
Tel Aviv, Israel
nadav@eng.tau.ac.il

***Abstract*—Weight windows are an important part of spectral analysis, especially in radar Doppler processing. Presently their study is in a stalemate, accepting the present tradeoff between mainlobe width and sidelobes attenuation as a fait accompli. An exception is Stankwitz et. al. Apodization technique for sidelobe reduction in SAR images. Our paper suggests an improved approach to windowing with performances expected from "Tri-Apodization" but with computational complexity of "Dual Apodization". The new approach achieves smaller SNR loss than a single low-sidelobes window. Basically the processor performs two FFTs following different windows and chooses the minimum at each output element. The predicted improved performances are confirmed by results from measured radar data.**

***Index Terms*—Weight windows, FFT, sidelobe reduction, Dolph-Chebyshev, Hamming, radar, Doppler response.**

I. Introduction

Weight windows [1-5] often precede FFT processing in order to reduce sidelobes (SL) level compared to the SL of a rectangular (uniform) window. The main drawback is widening of the mainlobe. A secondary disadvantage is an unavoidable loss in signal-to-noise ratio (SNR). In coherent radar processing, for example, FFT is usually performed on returns from many pulses, in order to obtain the Doppler shift of returns from a moving target at a given delay. Selecting the weight window and its parameters requires considering the tradeoff between mainlobe width and SL level. Present research on weight windows is limited to windows that provide a smooth tuning over the mainlobe/sidelobes tradeoff [6], or search for new windows that slightly improve the tradeoff [7]. An exception is Stankwitz et. al. Apodization technique for SL reduction in SAR images [8]. We propose here an improved processing approach with performances expected from "Tri-Apodization" but with computational complexity of "Dual Apodization" [8]. Namely, two FFTs are required, but not three. The resulted response suits radar processing due to its narrow mainlobe and low-level distant-SL. In between there remained two near-SL, at a tolerable level of -35dB.

II. Window Design

The design and processing involve two tracks (Fig. 1). In the left track a composite window is created from a linear combination of a rectangular window w_1,

$$w_1(n)=1,\ n=0,1,...,N-1 \tag{1}$$

And a medium performance window w_2, such as Hamming,

$$w_2(n)=\alpha+(1-\alpha)\cos\left(\frac{2\pi n}{N-1}\right),\ \alpha=0.54,\ n=0,1,...,N-1. \tag{2}$$

The resulted composite window is

$$w_{1,2}(n)=w_1(n)+\xi w_2(n),\ n=0,\ 1,...,\ N-1. \tag{3}$$

When w_2 is Hamming the optimal choice is $\xi=3.9$. What we mean by optimal will be explained when the resulted response is discussed.

Creating a new window from a linear combination of existing windows is not new. The Bartlett-Hann window [9] is a good example. The motivation there was exploiting the partially opposite signs of the SL, which caused SL reduction but maintained the mainlobe width. In our case the main result of the linear combination, which created $w_{1,2}$, is to achieve some reduction in near-SL height while maintaining a narrow mainlobe. The right track performs spectral analysis using a third classical window w_3, chosen for its very low and uniform SL.

The two tracks meet in front of a non-linear operation which, for each element, chooses the minimum of the responses of $w_{1,2}$ and w_3, after normalization. Namely, we first find the sum of the elements of each window,

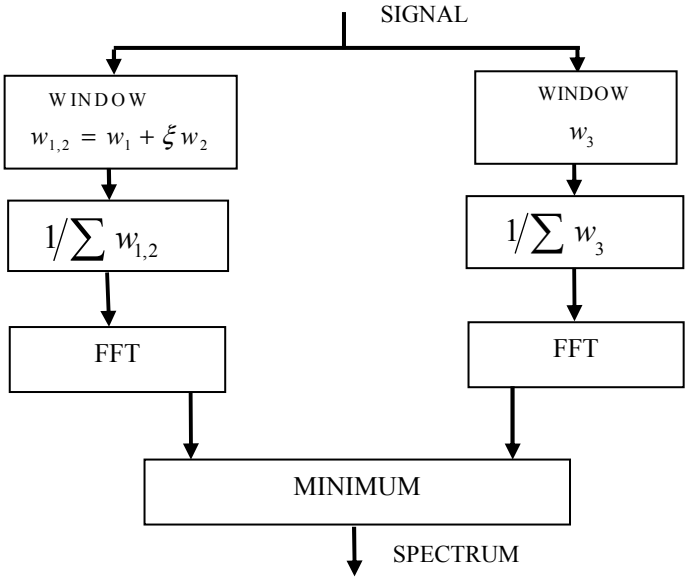

Fig. 1. Block diagram of the processor.

$$S_{1,2}=\sum_{n=0}^{N-1} w_{1,2}(n)\ ,\ \ S_3=\sum_{n=0}^{N-1} w_3(n)\ . \qquad (4)$$

We then perform two FFTs and choose the smaller of each normalized element of the two responses,

$$\left|W_{\min}(k)\right|=\min\left\{\frac{1}{S_{1,2}}\left|W_{1,2}(k)\right|,\frac{1}{S_3}\left|W_3(k)\right|\right\},\ 0\le k\le N-1\ , \qquad (5)$$

where $W_m(k)$ is the discrete Fourier transform (DFT) of the signal whose complex envelope is $u(n)$, when using a weight window $w_{\rm m}$:

$$W_m(k)=\sum_{n=0}^{N-1} w_m(n)u(n)\exp(-j2\pi kn/N),\ 0\le k\le N-1\ . \qquad (6)$$

To plot the response of the new window we set u(n) = 1 in (6). Fig. 2 presents the magnitude of the response (in dB) of the new window when w_2 is Hamming, $\xi = 3.9$ and w_3 is Dolph-Chebyshev with nominal SL level of -61dB. Also shown are a Dolph-Chebyshev response and a Hamming response. Note that Fig. 2 was obtained with N = 512, but only the first 6 elements of the response are shown.

The new window response contains 3 sections: (a) mainlobe whose width is approximately half way between the mainlobe widths of rectangular and Dolph-Chebyshev windows; (b) near SL whose height is in between the SL heights of the two windows; and (c) far SL almost identical to the far SL of Dolph-Chebyshev. Note the equal level (–35dB) of the two near SL; it was reached by controlling the coefficient ξ in (3).

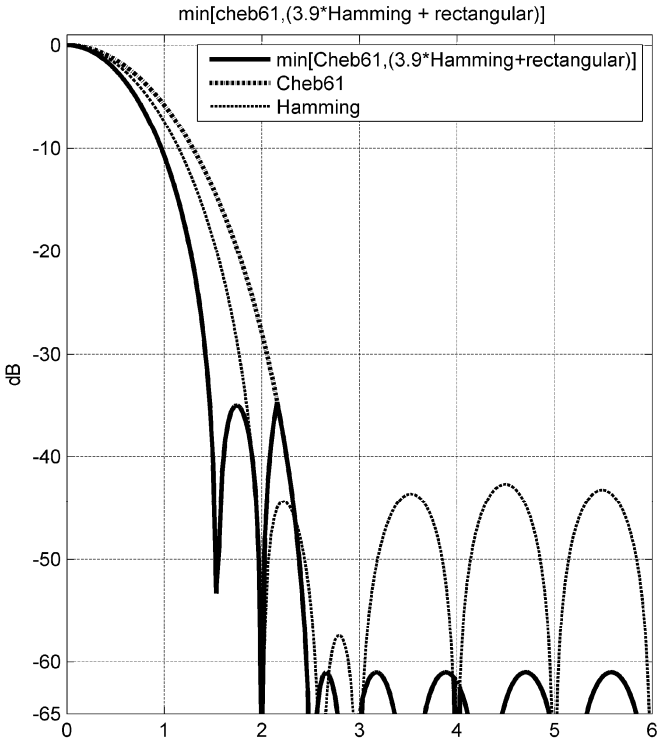

Fig. 2. Responses of the new window (solid), Dolph-Chebyshev, 61dB (dash-dot) and Hamming (dots), N=512.

The fact that the processing includes a non-linear operation raises a suspicion of non-linear effects in case additive noise or neighboring signals are present. In radar application a neighboring signal arrives from a second target, within the same azimuth-range cell, but having a different range-rate. The effects of noise or a neighbor signal were investigated by simulation.

Other w_2 partners to the rectangular window were tested, in particular another Dolph-Chebyshev, with $\xi = 1.7$, but Hamming yielded the most favorable near-SL pattern.

III. Two Signals

The new window was used with FFT spectrum calculation of two simulated CW signals at two different frequencies. The relative intensity and phase of the second signal were controlled. Fig. 3 presents the result for each signal by itself (top subplots) and the output when both signals are present (bottom subplot). Different relative intensities and phase differences were tried. All trials showed similar results, in which the spectrum of each signal was represented faithfully.

IV. Signal Plus Noise

The use of a weight window, other than a rectangular window, entails an SNR loss referred to as Loss Factor (*LF*). For conventional windows, in which the window elements $w(n)$ are defined, real and positive, the SNR loss is given [10] by

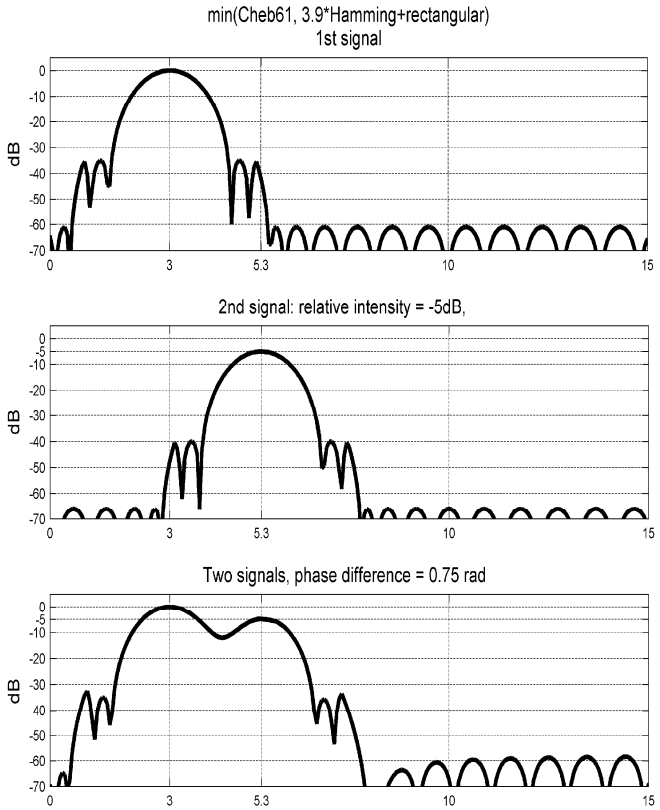

Fig. 3. Output from FFT, following the new weight window, of two CW signals at different frequencies: 1st signal (top), 2nd signal (middle), both signals (bottom).

$$LF = \frac{N\sum_{n=1}^{N} w^2(n)}{\left(\sum_{n=1}^{N} w(n)\right)^2},\quad LF_{\mathrm{dB}} = 10\log_{10}(LF). \qquad (7)$$

The new window cannot be described by a set of window elements, so its performances in the presence of noise and the loss factor were calculated using Monte-Carlo simulations. For a given noise level and a specified probability of false alarm, P_{FA}=0.001, the required detection threshold were found for each weight window. When a CW signal was added, and using each window's threshold, the SNR was raised until the specified probability of detection P_D=0.8 was reached. The results are listed in Table I.

Table I compares the new window with a Dolph-Chebyshev window, for which both theoretical, simulation and experimental results are available. The agreement between theory and simulation in the Dolph-Chebyshev case confirms the viability of the simulation approach for calculating LF. An interesting and important result is that the new window exhibits SNR loss (0.9dB) that is less than the Dolph-Chebyshev loss (1.85dB), and greater than the composite window loss (0.67dB). In other words, the loss is in-between the individual losses of the windows in the two tracks.

TABLE I.

	SNR Loss, N=512, P_{FA}=0.001, P_D=0.8			
Window	*LF [dB], Simul.*	*LF [dB], Theory*	*LF [dB], Theory*	*LF [dB], Measure*
N	512		2048	
w_1, Rectangular	0	0	0	0
w_3, Chebwin(N,61)	1.8	1.851	1.846	1.55
$w_{1,2}$, Composite		0.673	0.671	
New window	0.9	?	?	0.73

Fig. 4 The alley of scene 1.

V. Results From An Experimental Radar – Scene 1

Three windows: Rectangular, Dolph-Chebyshev and the new window, were compared when processing the same target returns, recorded by experimental Bistatic CW radar. The coherent processing interval (CPI) contained 2048 periods of the periodic waveform. The radar scene was an alley in which several cars were receding slowly away from the roof of a 4-story building, where the radar transmitter and receiver were co-located. The alley is shown in Fig. 4. The antennas' beamwidths were too wide to provide a meaningful azimuth resolution. At each range slot the processor performed an FFT of 2048 elements to yield a range-Doppler display. The entire processing was repeated three times, using the three windows. Zooms on a small section of the range/range-rate displays, using the three windows, are presented in Figs. 5 to 7. The color bar represents intensities in dB. The full display span (not shown) is $0 \le R \le 4000\mathrm{m}$, $-320 \le \dot{R} \le 320\mathrm{m/s}$.

The displays reveal ten cars moving at range-rates between 6 and 9 m/s, within a range span of 50 to 250m. Fig. 5 was obtained with a rectangular weight window (N=2048). Zero padding increased the FFT size to M=8192 elements. Strong range-rate SL are evident in Fig. 5, as expected from a rectangular window. Fig. 6 was obtained with a Dolph-Chebyshev window designed for –60dB SL. The dynamic intensity span of the scene is too limited to show the –60dB range-rate SL, but when comparing with Fig. 5, the widening of the mainlobes is evident. Fig. 7 was obtained with the proposed new window. Here too the –60dB range-rate far-SL are too low to be seen. Careful observation of Fig. 7 shows narrower mainlobes than in Fig. 6. The two –35dB near-SL, on each side, are barely visible. The markers on the most distant target show the intensity obtained in the processed measurements (161.25, 159.7, 160.52dB). The LF results, deduced from the markers, appear in the last column of Table I and match theory and simulations. The three drawings with real radar measurements demonstrate the advantage of the new window – very low SL without sacrifices in mainlobe width and loss. This is very important when a weak target is close in Doppler to strong clutter.

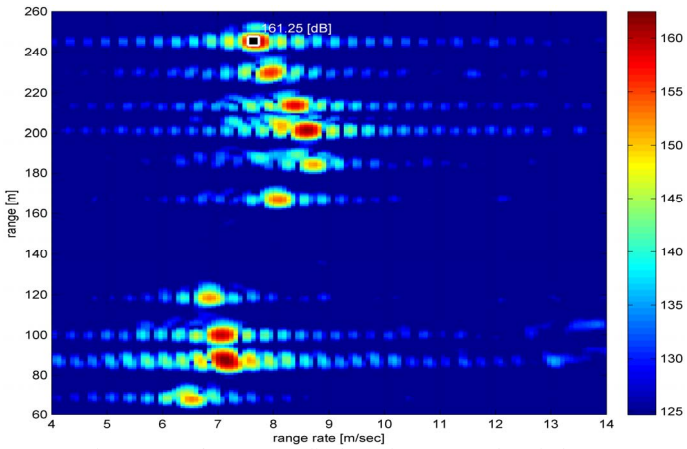

Fig. 5. Range/Range-rate display using rectangular window. Color bar scale in dB. (Same in all following Figs.)

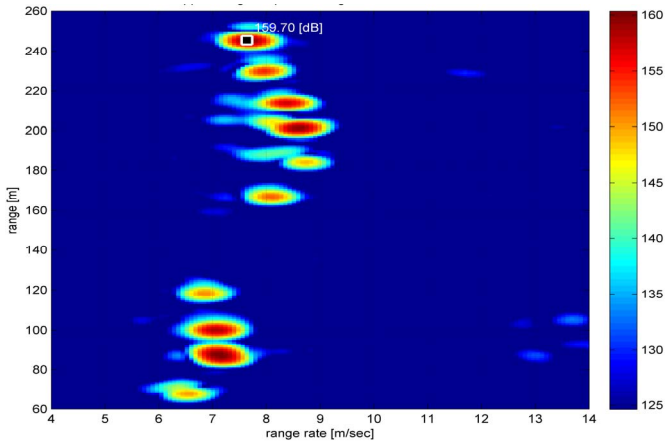

Fig. 6. Range/Range-rate display using Dolph-Chebyshev window.

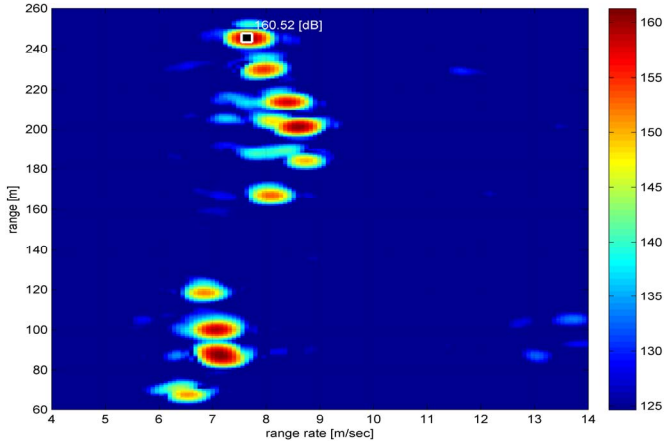

Fig. 7. Range/Range-rate display using the new window.

While not related to our topic, we point out that the lack of range SL in Figs. 5 to 7 is due to the use of a periodic waveform exhibiting perfect periodic autocorrelation.

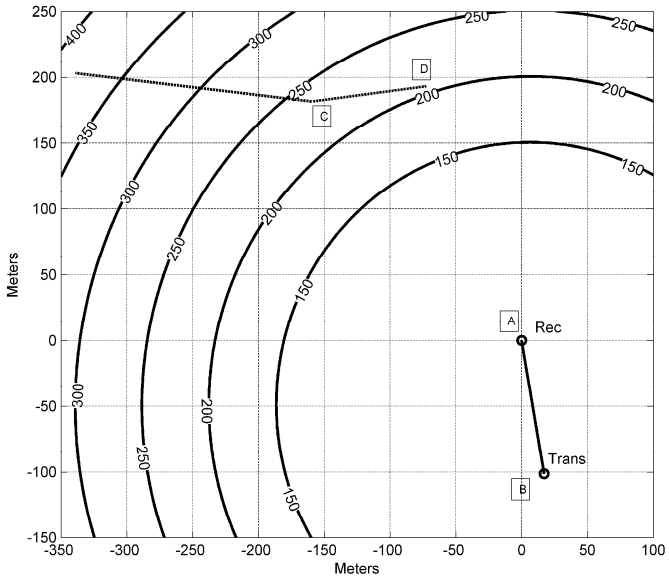

Fig. 8. Scene 2. Area map with bi-static radar locations and road section

Fig. 9. The four inbound cars in scene 2.

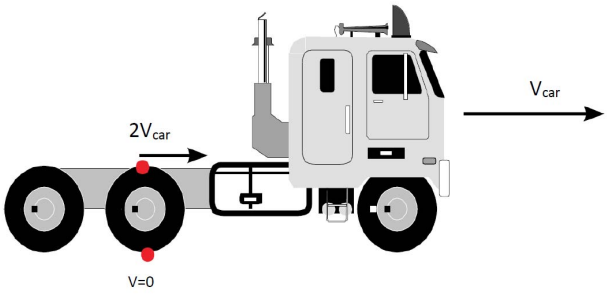

Fig. 10. Wheel velocities in a moving car

VI. Results From An Experimental Radar – Scene 2

The second scene was a true bi-static scene, depicted in Fig. 8. The baseline length was 103m. The contour labels are of the bi-static range:

$$\text{contour value} = \frac{1}{2}\left(R_{\text{target}-\text{trans}} + R_{\text{target}-\text{rec}} - b\right) \qquad (8)$$

$$\text{baseline}: b = R_{\text{trans}-\text{rec}}$$

The inbound lane has a guard rail which ends near point C. Thus, wheels of cars located further from the radar than point C will be eclipsed. The targets in scene 3 are four inbound cars (Fig. 9). Only the wheels of the closest car (black van) are not obscured by the rail. Fig. 10 demonstrates that the span of horizontal velocities of a wheel extends from zero to twice the car speed.

The radar displays (Figs. 11 and 12) clearly show four major scaterrers at bi-static ranges of: 240, 280, 305 and 340 meters, which are believed to represent the four cars.

The closest scaterrer, at 240m is associated with the black van, whose wheels are not obscured by the guard rail. This explains the span of reflections at bistatic range-rates extending on both sides of the car body reflection, whose bistatic range-rate is –14m/s. The reflections with the higher velocities (–25 to –14m/s) are stronger because they come from the upper sections of the wheels. The reflections with the lower velocities (–14 to –6m/s) are weaker because they come from the lower sections of the wheels and are also attenuated by the MTI cancellers used by the Doppler processor.

The fine structure of the wheels' micro-Doppler returns provides a good opportunity to compare the two weight windows. Fig. 11 was obtained with the new window and Fig. 12 was obtained with a classical Dolph-Chebyshev (-60 dB) window. First note that the car body is represented by two strong scaterrers (bistatic range-rates ≈ –14m/s) which are better separated in Fig. 11. Better separated (also in Fig. 16) are the three strong wheels' reflections at bistatic range-rates

of –16, –17 and –18m/s. While not marked on the drawings, the intensities of the peaks in Fig. 11 are approximately 0.8dB stronger than the corresponding peaks in Fig. 12.

VII. Conclusions

A new weight window is proposed, to be used in front of FFT processing. The processing involves (a) a first FFT using a window which is a linear combination of two classical windows (rectangular and Hamming), (b) a second FFT using a Dolph-Chebyshev window, and (c) a "minimum" operation between the two FFT outputs.

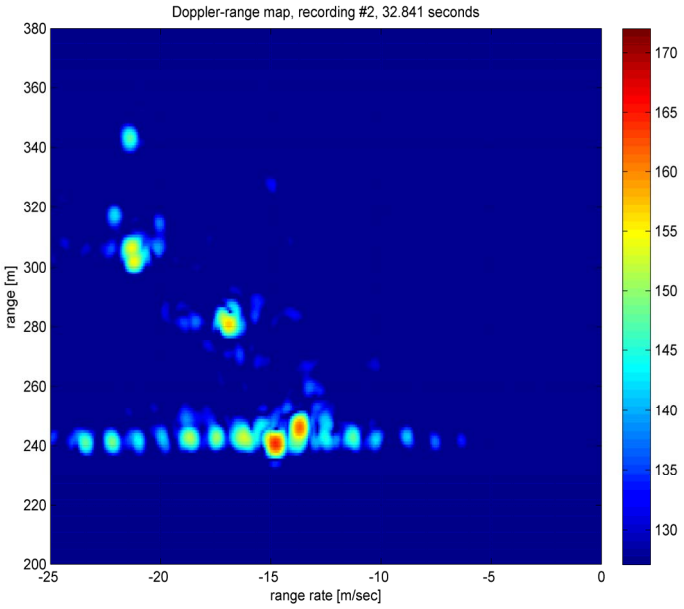

Fig. 11. Range vs. range-rate radar display of the four inbound cars in scene 2, using the new weight window.

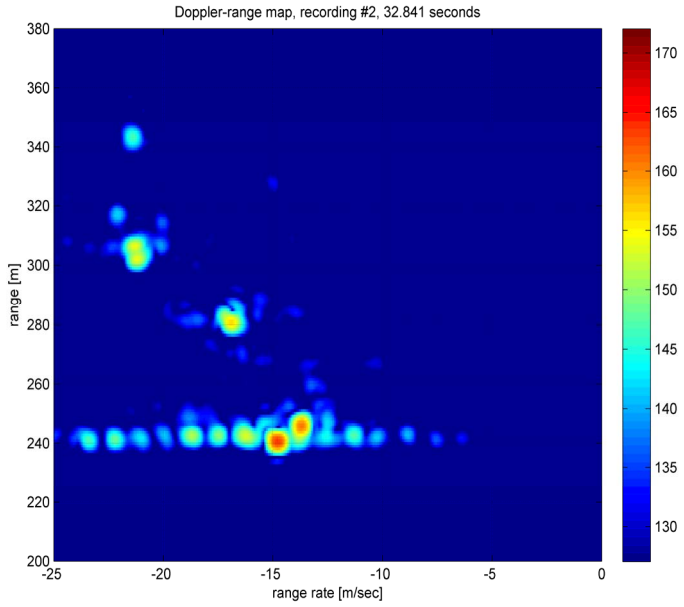

Fig. 12. Range vs. range-rate radar display of the four inbound cars in scene 2, using Chebwin(N,60) window.

The new window yields narrow mainlobe and low SL. Its SNR loss is almost 1 dB smaller than the SNR loss of a Dolph-Chebyshev window alone. No ill effects were observed as a result of the non-linear "minimum" operation, in the presence of additional signals and noise. The main drawback is the need to perform two FFTs instead of one. The improved properties of the new window were confirmed in simulations and with real radar data.

References

[1] F. J. Harris, "On the use of Windows for harmonic analysis with the discrete Fourier transform," IEEE Proc., vol. 68, no. 1, pp. 51-83, Jan. 1978.

[2] B. Porat, A Course in Digital Signal Processing. New York, NY, USA: Wiley, 1997.

[3] A. Antoniou, Digital Signal Processing: Signals, Systems, and Filters. New York, NY, USA: McGraw-Hill, 2005.

[4] S. Rapuano, and F. J. Harris, "An introduction to FFT and time domain windows," IEEE Instrum. Meas. Mag., vol. 10, no. 6, pp. 32-44, Dec. 2007.

[5] K. M. M. Prabhu, Window Functions and Their Applications in Signal Processing. Boca Raton, FL, USA: CRC Press, 2014.

[6] C. M. Zierhofer, "Data window with tunable sidelobe ripple decay," IEEE Signal Process. Lett., vol. 14, no. 11, pp.824-827, Dec. 2007.

[7] M. Mottaghi-Kashtiban, and M. G. Shayesteh, "New efficient window function, replacement for the Hamming window," IET Signal Process., vol. 5, no. 5, pp. 499-505, Aug. 2011.

[8] H.C. Stankwitz, R. J. Dallaire and J. R. Fienup, "Nonlinear Apodization for sidelobe control in SAR imagery," IEEE Trans. Aerospace and Electronic Systems, vol. 31, no. 1, pp. 267-279, Jan. 1995.

[9] Y. H. Ha, and J. A. Pearce, "A new window and comparison to standard windows," IEEE Trans. Acoust., Speech, Signal Process., vol. 37, no. 2, pp. 298-301, Feb. 1989.

[10] H. Urkowitz, J. D. Geisler, and N. A. Ricciardi, JR., "The effect of weighting upon signal-to-noise ratio in pulse bursts," IEEE Trans. Aerospace and Electronic Systems, vol. 9, no. 4, pp. 486-494, Jul. 1973.